Author Manuscript

Author Manuscript

Author Manuscript

Author Manuscript

HHS Public Access

Author manuscript

J Am Chem Soc. Author manuscript; available in PMC 2021 February 17.

Published in final edited form as:

J Am Chem Soc. 2020 February 05; 142(5): 2115–2119. doi:10.1021/jacs.9b09985.

Observation of the Imidazole-Imidazolium Hydrogen Bonds Responsible for Selective Proton Conductance in the Influenza A M2 Channel

Riqiang Fu

National High Magnet Field Lab, Tallahassee, Florida 32310, United States

Yimin Miao, **Huajun Qin**

Department of Chemistry and Biochemistry, Florida State University, Tallahassee, Florida 32306, United States

Timothy A. Cross

National High Magnet Field Lab, Tallahassee, Florida 32310, United States; Department of Chemistry and Biochemistry, Florida State University, Tallahassee, Florida 32306, United States

Abstract

The integral membrane M2 protein is a 97-residue membrane protein that assembles as a tetramer to conduct protons at a slow rate (10^2–10^3/s) when activated by low pH. The proton conductance mechanism has been extensively debated in the literature, but it is accepted that the proton conductance is facilitated by hydrogen bonds involving the His37 residues. However, the hydrogen bonding partnership remains unresolved. Here, we report on the measurement of ^{15}N–^{15}N *J*-couplings of ^{15}N His37-labeled full length M2 (M2FL) protein from *Influenza A* virus embedded in synthetic liquid crystalline lipid bilayers using two-dimensional *J*-resolved NMR spectroscopy. We experimentally observed the hydrogen-bond mediated *J*-couplings between $N_{\delta 1}$ and $N_{\varepsilon 2}$ of adjacent His37 imidazole rings, providing direct evidence for the existence of various imidazolium-imidazole hydrogenbonding geometries in the histidine tetrad at low pH, thus validating the proton conduction mechanism in the M2FL protein by which the proton is transferred through the breaking and reforming of the hydrogen bonds between pairs of His37 residues.

The M2 protein from the *Influenza A* virus is a 97-residue membrane protein with a 24-residue N-terminal and a 51-residue C-terminal segment connected by a single trans-membrane (TM) helix of 22 residues. It assembles as a tetrameric bundle to form a channel

Corresponding Author: **Riqiang Fu** – National High Magnet Field Lab, Tallahassee, Florida 32310, United States; rfu@magnet.fsu.edu.

Supporting Information

The Supporting Information is available free of charge at https://pubs.acs.org/doi/10.1021/jacs.9b09985.

Materials and experimental details; 1D ^{15}N CPMAS spectrum of the His37-labeled M2FL sample; 1D spectra taken along the F1 dimension of the 2D *J*-resolved spectrum in Figure 3; demonstration for the double spin–echo sequence used for *J*-refocusing and the full doubly spin–echoed spectra of the M2FL sample at different echo times (PDF)

Complete contact information is available at: https://pubs.acs.org/10.1021/jacs.9b09985

The authors declare no competing financial interest.

Author Manuscript Author Manuscript Author Manuscript Author Manuscript

that is activated at low pH to conduct protons at a slow rate ($10^2 - 10^3$/s), essential for the viral life cycle.[1,2] The α-helical TM domain (residues 25–46) is responsible for proton conductance triggering the release of viral RNA into the host cells. This tetrameric TM domain is an important drug target.[3–6] The four His37 residues reside near the center of the TM helix and are known to be the heart of the proton conducting channel, the key to the proton transport mechanism.[7] Several different constructs reconstituted in various lipid environments have been the subject of intensive high-resolution structural studies in the past decade using both magic-angle-spinning (MAS)[8–15] and oriented sample[3,16–19] solid-state NMR, as well as solution NMR[20–23] and X-ray crystallography.[24,25] It has been clear so far that the proton conductance in the M2 channel is facilitated through hydrogen bonds with the His37 residues. But two possible models for His37 hydrogen bonding partners have been presented and debated in the literature (Figure 1). The imidazolium-imidazole bonding of His-His$^+$ pairs (c.f. Figure 1a) that form low-barrier hydrogen bonds (LBHB) as previously suggested with ^{1}H frequencies as high as 18.7 ppm and protonated ^{15}N frequencies as high as 195 ppm; i.e., the proton is transferred through protonating the τ state of one His-His$^+$ pair to form a +3 state for the His tetrad prior to deprotonation and reforming the +2 state of the His tetrad.[7,17,26] If the His37 residue does not form His-His hydrogen bonded pairs, but only hydrogen bonds with water (cf. Figure 1b), a proton shuttling mechanism is proposed; i.e., the His37 shuttles protons through imidazole ring reorientations and exchanging protons with water without forming an intermonomer hydrogen bond between the His37 residues.[27–29]

To support the shuttling mechanism, two-dimensional (2D) ^{1}H–^{15}N heteronuclear correlation (HETCOR) experiments were performed to see if there were any correlations between the water protons and the nitrogens in the His37 side chains. It has been shown in the ^{1}H–^{15}N HETCOR spectra[28] of an M2 transmembrane construct, M2(22–46), in a virus-envelopemimetic lipid membrane that the ^{15}N peaks were in the range 160–180 ppm, correlating to ^{1}H chemical shifts of 8–12 ppm, similar to a typical backbone amide ^{1}H chemical shift range, and correlating to the 1H peak of water at ~5 ppm. No imidazole-imidazolium cross peaks were observed in the ^{13}C–^{13}C correlation spectra of the +2 charged state of M2(22–46).[27] However, the correlated peaks between ^{15}N and water protons can arise either from direct water-His proton transfer (cf. Figure 1b) or from additional protonation to form a transient +3 state for the His tetrad prior to deprotonation, potentially from a water in the viral interior (i.e., indirect transfer through the chemical exchange between hydronium ions and the protons of the histidine side chain NH bonds),[26] as illustrated in Figure 1a. Recently, more experimental evidence has been obtained as alluded to above from the full length M2 (M2FL) protein in lipid bilayers that support the LBHB model: (i) both high ^{1}H and ^{15}N frequencies extend up to 19 and 190 ppm, respectively, in the 2D ^{1}H–^{15}N HETCOR spectra, and the nonprotonated ^{15}N resonances extending from 250 ppm down to 235 ppm—such extreme frequencies clearly indicate the formation of short imidazole-imidazolium hydrogen bonds in the His37 tetrad;[26,30] (ii) the observation that the hydronium ions are in chemical exchange on a submsec time scale with the protons of the imidazole-imidazolium hydrogen bonds;[31] (iii) the observations of ^{13}C–^{13}C and ^{15}N –^{15}N chemically exchange cross peaks between His37 residues in the neutral and charged states;[32] and (iv) no evidence for the π state under even mild acidic pH conditions when

Author Manuscript Author Manuscript Author Manuscript Author Manuscript

characterizing the full length protein.[26] Nevertheless, these results may still be considered as indirect evidence to affirm the LBHB model. Here, we seek direct and definitive evidence for the imidazole-imidazolium hydrogen bonding partner by measuring through-bond scalar coupling, i.e. *J*-coupling, between the two nitrogen sites.

A hydrogen bond is primarily an electrostatic attraction between two polar groups containing highly electronegative atoms such as nitrogen, oxygen, and fluorine that are bridged by a hydrogen atom. However, charge transfer (covalency) and dispersive energies are also important, especially when considering strong hydrogen bonds.[33] It has been well-known that the electron sharing within covalent bonds results in *J*-couplings. Similarly, the redistribution of electron densities upon hydrogen bond formation acts as electron sharing between the two nuclei involved in the hydrogen bond, although they are not covalently bonded.[34] As a result, there exist hydrogen-bond mediated *J*-couplings between the two electronegative atoms involved.[35] Such *J*-couplings across the hydrogen bonds have been observed in both solution[36–40] and solid-state NMR[41–43] spectra and are considered as a direct detection of hydrogen bonds. Here, the LBHB model (cf. Figure 1a) involves two electronegative nitrogen atoms, one of which is protonated; thus, there should exist homonuclear hydrogen-bond mediated $^{15}N–^{15}N$ *J*-couplings $^{2h}J(N_{\delta 1}\cdots H\cdots N_{\varepsilon 2})$ between the two involved nitrogen atoms. In the water-His37 hydrogen bonding model (cf. Figure 1b), the two involved electronegative atoms are nitrogen and oxygen, meaning that there should be heteronuclear hydrogen-bond mediated $^{15}N–^{17}O$ *J*-couplings between the nitrogen and oxygen, but not homonuclear $^{15}N–^{15}N$ *J*-couplings. Therefore, we use ^{15}N 2D *J*-resolved spectroscopy in high-resolution solid-state NMR to differentiate the hydrogen bonding partners at the heart of the His37 tetrad of the M2FL proton channel.

As demonstrated in the literature,[41] the rotor-synchronized spin–echo (CP − $t_1/2$ − π − $t_1/2$ − t_2) sequence can be used to measure homonuclear *J*-couplings, where CP stands for cross-polarization from ^1H to ^{15}N, t_1 and t_2 represent the time evolution in the indirect and observed dimension, respectively, where $t_1/2$ has to be set to a multiple of spinning periods. High power ^1H decoupling is applied during the entire t_1 and t_2 dimensions. Because there are two nitrogen sites in the imidazole ring of histidine separated by two covalent bonds, we need to first examine whether or not there exists a two-bond *J*-coupling (i.e., $^2J(N_{\delta 1}\cdots N_{\varepsilon 2})$) between these two nitrogen atoms. Figure 2 shows the ^{15}N 2D *J*-resolved spectrum for the histidine sample lyophilized from a pH 6.3 solution. At this pH, there are two tautomeric states, the neutral τ state and the charged state; the π state is not present at this pH.[44] From the slices in the right panel, it is clear that the protonated ^{15}N sites (especially $N_{\varepsilon 2}$) have a slightly broader line width (~9 Hz) than the nonprotonated ^{15}N site (~7 Hz), owing to some residual $^1H–^{15}N$ interactions for the protonated ^{15}N sites that are not fully refocused by the spin echo sequence. Nevertheless, no *J*-splitting is observed for the histidine sample, implying that there is no detectable $^2J(N_{\delta 1}\cdots N_{\varepsilon 2})$ between the $N_{\delta 1}$ and $N_{\varepsilon 2}$ sites that are separated by two chemical bonds in the imidazole rings for both charged and neutral τ states.

Figure S1 shows the ^{15}N CPMAS NMR spectrum of the His37-labeled M2FL ($H_{57,90}Y$, pH 6.2) in DOPC/DOPE liposomes. It is noteworthy that, in the uniform ^{13}C and ^{15}N labeling media for this protein expression, unlabeled Phe, Tyr, and Trp amino acids were added to the

Author Manuscript Author Manuscript Author Manuscript Author Manuscript

bacterial cultures to suppress these aromatic amino acid resonances. Therefore, the observed signals from 150 to 260 ppm, as shown in the expanded spectrum in Figure S1 and in refs 26, 31, and 32 are solely from the His37 tetrad. Furthermore, it is important to emphasize that the M2 spectra display a broad distribution of ^{15}N chemical shifts for both the protonated and nonprotonated ^{15}N His37 side chain resonances.[26] These resonances have been shown to be heterogeneously and not homogeneously broadened.[26,32] In addition, the heterogeneity largely results from transmembrane helix–helix packing. This proton channel is formed by a tetramer of a single transmembrane helix, and unlike many transmembrane proteins that have small residues at the helix–helix interface, M2 has large side chains, such as Leu38, that can take on different χ_2 rotameric states resulting in slightly different ^{15}N $-^{15}$N distances for the imidazole-imidazolium hydrogen bonded state leading to the broad distribution of the ^{15}N, ^{13}C, and ^{1}H chemical shifts observed for His37.[26,32] Such heterogeneity may be the key to the instability of the imidazole-imidazolium hydrogen bonds that permit proton conductance, albeit on the very slow millisecond time scale. Such a slow time scale is not explained by the mechanism illustrated in Figure 1b.

Figure 3 shows the ^{15}N 2D *J*-resolved spectrum of the His37-labeled M2FL protein at pH 6.2 in DOPC/DOPE liposomes together with extracted rows at specific ^{15}N chemical shifts. The natural line width for all ^{15}N chemical shift positions from 165 to 190 ppm appears to be ~60 Hz. This implies, as described above, that the broad ^{15}N resonance bands observed from 165 to 190 ppm are the result of inhomogeneous broadening, a distribution of chemically distinguishable His37 conformations, rather than exchange broadening at a rate comparable to the chemical shift difference between the protonated and nonprotonated $N_{\delta 1}$ and $N_{\varepsilon 2}$ sites. The slices through the 2D data set (Figure 3) do not have enough sensitivity owing to having just four $^{15}N_{\delta 1}$ and four $^{15}N_{\varepsilon 2}$ sites whose signals are each spread over more than 25 ppm between 160 and 200 ppm in this full length protein in liquid crystalline lipid bilayers. But the transverse dephasing times (T'_2)[45] from fittings (Figure 3) decrease steadily at a higher ppm position, all shorter than that of the amide nitrogen (Figure S2). Such a decrease in T'_2 could indicate the presence of *J*-coupling (eq S1). It is known that the homonuclear *J*-coupling can be refocused by applying a $\pi/2$ pulse in the middle of double spin-echoes (Figure S3).[46,47] Figure 4 shows the doubly spin-echoed ^{15}N spectra of the M2FL sample with and without *J*-refocusing. At t_1 = 20.48 ms, the *J*-refocused signals (in red) from 170 to 185 ppm are consistently higher than those (in black) without applying the $\pi/2$ pulse, as clearly indicated by the integration curve (blue). These results document the existence of $^{2h}J(N_{\delta 1}\cdots H\cdots N_{\varepsilon 2})$ as suggested previously through the $^{15}N-^{1}H$ correlation spectra with ^{1}H frequencies up to 18.7 ppm and ^{15}N frequencies up to 195 ppm.[26] Using t_1 = 32.0 ms, the *J*-refocused signal at 174 ppm had a much higher intensity (above the noise level) than without the *J*-refocusing, whose ratio yielded a $^{2h}J(N_{\delta 1}\cdots H\cdots N_{\varepsilon 2})$ value of 8.1 Hz from eqs S1 and S2, which represents typical $^{2h}J(N\cdots H\cdots N)$ values observed in other compounds.[41–43] This confirms the existence of imidazole-imidazolium hydrogen bonds in the His37 tetrad of the M2 protein, since the control spectrum (Figure 2) indicates no two-bond *J*-coupling between the $N_{\delta 1}$ and $N_{\varepsilon 2}$ sites within the imidazole ring. The further decrease in the T'_2 values at the higher ^{15}N chemical shifts might indicate a larger $^{2h}J(N_{\delta 1}\cdots H\cdots N_{\varepsilon 2})$ and thus could imply stronger hydrogen bonds as the protonated ^{15}N chemical shift moves to lower field.[26,32] Thus, the large $^{2h}J(N_{\delta 1}\cdots H\cdots N_{\varepsilon 2})$ values

Author Manuscript Author Manuscript Author Manuscript Author Manuscript

hypothesized here are consistent with the observation of high ^{1}H and ^{15}N chemical shifts observed in the $^{1}H-^{15}N$ HETCOR spectra for the same sites, all reflecting on the broad range of the imidazole-imidazolium hydrogen-bond strengths in the His37 tetrad.[26,30,32] These relatively infrequent strong hydrogen bonds may be responsible for the low M2 proton conductance rate. Furthermore, this range of *J*-couplings and chemical shifts is consistent with the explanation that packing of various large hydrophobic side chains in the helix–helix interface results in a subtle range of distances between the imidazole and imidazolium side chains due to slight shifts in the $C\alpha-C\alpha$ separation of the backbone.[26]

To conclude, we used the 2D *J*-resolved NMR spectrum to measure the hydrogen-bond mediated $^{15}N-^{15}N$ *J*-couplings at the heart of the His37 tetrad of the M2 protein. The observed $^{2h}J(N_{\delta 1}\cdots H\cdots N_{\varepsilon 2})$ provides direct observation of the heterogeneous imidazole-imidazolium hydrogen bonds in the His37 tetrad of the M2 protein, thus validating the LBHB proton conductance mechanism at the heart of the M2FL proton channel. Furthermore, these *J*-couplings are highly correlated with distributions of chemical shifts, as in disordered solids,[48,49] and could be used to refine detailed local structural models in such heterogeneous environments through theoretical calculations.[35,50]

Supplementary Material

Refer to Web version on PubMed Central for supplementary material.

ACKNOWLEDGMENTS

This work was supported by NIH Grants AI023007 and AI119178. All NMR experiments were carried out at the National High Magnetic Field Lab (NHMFL) supported by the NSF Cooperative Agreement DMR-1644779 and the State of Florida.

REFERENCES

(1). Sugrue RJ; Hay AJ Structural characteristics of the M2 protein of influenza-A viruses - evidence that it forms a tetrameric channel. Virology 1991, 180, 617. [PubMed: 1989386]

(2). Sakaguchi T; Tu QA; Pinto LH; Lamb RA The active oligomeric state of the minimalistic influenza virus M-2 ion channel is a tetramer. Proc. Natl. Acad. Sci. U. S. A 1997, 94, 5000. [PubMed: 9144179]

(3). Hu J; Asbury T; Achuthan S; Li C; Bertram R; Quine JR; Fu R; Cross TA Backbone structure of the amantadine-blocked trans-membrane domain M2 proton channel from influenza A virus. Biophys. J 2007, 92, 4335. [PubMed: 17384070]

(4). Nishimura K; Kim SG; Zhang L; Cross TA The closed state of a H+ channel helical bundle combining precise orientational and distance restraints from solid state NMR. Biochemistry 2002, 41, 13170. [PubMed: 12403618]

(5). Lamb RA; Zebedee SL; Richardson CD Influenza virus-M2 protein is an integral membrane-protein expressed on the infected-cell surface. Cell 1985, 40, 627. [PubMed: 3882238]

(6). Grambas S; Bennett MS; Hay AJ Influence of amantadine resistance mutations on the pH regulatory function of the M2-protein of influenza-A viruses. Virology 1992, 191, 541. [PubMed: 1448912]

(7). Hu J; Fu R; Nishimura K; Zhang L; Zhou HX; Busath DD; Vijayvergiya V; Cross TA Histidines, heart of the hydrogen ion channel from influenza A virus: Toward an understanding of conductance and proton selectivity. Proc. Natl. Acad. Sci. U. S. A 2006, 103, 6865. [PubMed: 16632600]

Author Manuscript Author Manuscript Author Manuscript Author Manuscript

(8). Miao Y; Qin H; Fu R; Sharma M; Can TV; Hung I; Luca S; Gor'kov PL; Brey WW; Cross TA M2 Proton Channel Structural Validation from Full-Length Protein Samples in Synthetic Bilayers and *E. coli* Membranes. Angew. Chem 2012, 124, 8508.

(9). Can TV; Sharma M; Hung I; Gor'kov PL; Brey WW; Cross TA Magic Angle Spinning and Oriented Sample Solid-State NMR Structural Restraints Combine for Influenza A M2 Protein Functional Insights. J. Am. Chem. Soc 2012, 134, 9022. [PubMed: 22616841]

(10). Cady SD; Schmidt-Rohr K; Wang J; Soto CS; DeGrado WF; Hong M Structure of the amantadine binding site of influenza M2 proton channels in lipid bilayers. Nature 2010, 463, 689. [PubMed: 20130653]

(11). Cady SD; Mishanina TV; Hong M Structure of amantadine-bound M2 transmembrane peptide of influenza A in lipid bilayers from magic-angle-spinning solid-state NMR: the role of Ser31 in amantadine binding. J. Mol. Biol 2009, 385, 1127. [PubMed: 19061899]

(12). Andreas LB; Eddy MT; Pielak RM; Chou JJ; Griffin RG Magic angle spinning NMR investigation of Influenza A $M2_{18–60}$: Support for an allosteric mechanism of inhibition. J. Am. Chem. Soc 2010, 132, 10958. [PubMed: 20698642]

(13). Andreas LB; Eddy MT; Chou JJ; Griffin RG Magic-angle-spinning NMR of the drug resistant S31N M2 proton transporter from Influenza A. J. Am. Chem. Soc 2012, 134, 7215. [PubMed: 22480220]

(14). Colvin MT; Andreas LB; Chou JJ; Griffin RG Proton association constants of His 37 in the Influenza-A M218–60 dimerof-dimers. Biochemistry 2014, 53, 5987. [PubMed: 25184631]

(15). Andreas LB; Reese M; Eddy MT; Gelev V; Ni QZ; Miller EA; Emsley L; Pintacuda G; Chou JJ; Griffin RG Structure and mechanism of the Influenza A M218–60 Dimer of Dimers. J. Am. Chem. Soc 2015, 137, 14877. [PubMed: 26218479]

(16). Du J; Cross TA; Zhou HX Recent progress in structure-based anti-influenza drug design. Drug Discovery Today 2012, 17, 1111. [PubMed: 22704956]

(17). Sharma M; Yi M; Dong H; Qin H; Peterson E; Busath DD; Zhou HX; Cross TA Insight into the mechanism of the influenza A proton channel from a structure in a lipid bilayer. Science 2010, 330, 509. [PubMed: 20966252]

(18). Wang J; Wu Y; Ma C; Fiorin G; Wang J; Pinto LH; Lamb RA; Klein ML; Degrado WF Structure and inhibition of the drug-resistant S31N mutant of the M2 ion channel of influenza A virus. Proc. Natl. Acad. Sci. U. S. A 2013, 110, 1315. [PubMed: 23302696]

(19). Wang JF; Kim SG; Kovacs F; Cross TA Structure of the transmembrane region of the M2 protein H+ channel. Protein Sci. 2001, 10, 2241. [PubMed: 11604531]

(20). Schnell JR; Chou JJ Structure and mechanism of the M2 proton channel of influenza A virus. Nature 2008, 451, 591. [PubMed: 18235503]

(21). Pielak RM; Schnell JR; Chou JJ Mechanism of drug inhibition and drug resistance of influenza A M2 channel. Proc. Natl. Acad. Sci. U. S. A 2009, 106, 7379. [PubMed: 19383794]

(22). Pielak RM; Oxenoid K; Chou JJ Structural investigation of rimantadine inhibition of the AM2-BM2 chimera channel of influenza viruses. Structure 2011, 19, 1655. [PubMed: 22078564]

(23). Pielak RM; Chou JJ Solution NMR structure of the V27A drug resistant mutant of influenza A M2 channel. Biochem. Biophys. Res. Commun 2010, 401, 58. [PubMed: 20833142]

(24). Stouffer AL; Acharya R; Salom D; Levine AS; Di Costanzo L; Soto CS; Tereshko V; Nanda V; Stayrook S; DeGrado WF Structural basis for the function and inhibition of an influenza virus proton channel. Nature 2008, 451, 596. [PubMed: 18235504]

(25). Acharya R; Carnevale V; Fiorin G; Levine BG; Polishchuk AL; Balannik V; Samish I; Lamb RA; Pinto LH; DeGrado WF; Klein ML Structure and mechanism of proton transport through the transmembrane tetrameric M2 protein bundle of the influenza A virus. Proc. Natl. Acad. Sci. U. S. A 2010, 107, 15075. [PubMed: 20689043]

(26). Miao Y; Fu R; Zhou HX; Cross TA Dynamic short hydrogen bonds in histidine tetrad of full length M2 proton channel reveal tetrameric structural heterogeneity and functional mechanism. Structure 2015, 23, 2300. [PubMed: 26526851]

(27). Hu F; Schmidt-Rohr K; Hong M NMR Detection of pH-Dependent Histidine-Water Proton Exchange Reveals the Conduction Mechanism of a Transmembrane Proton Channel. J. Am. Chem. Soc 2012, 134, 3703. [PubMed: 21974716]

Author Manuscript Author Manuscript Author Manuscript Author Manuscript

(28). Hong M; Fritzsching KJ; Williams JK Hydrogen-Bonding Partner of the Proton-Conducting Histidine in the Influenza M2 Proton Channel Revealed From ^{1}H Chemical Shifts. J. Am. Chem. Soc 2012, 134, 14753. [PubMed: 22931093]

(29). Liang R; Li H; Swanson JMJ; Voth GA Multiscale simulation reveals a multifaceted mechanism of proton permeation through the influenza A M2 proton channel. Proc. Natl. Acad. Sci. U. S. A 2014, 111, 9396. [PubMed: 24979779]

(30). Eckert H; Yesinowski JP; Silver LA; Stolper EM Water in silicate glasses: Quantitation and structural stidies by proton solid echo and magic angle spinning NMR methods. J. Phys. Chem 1988, 92, 2055.

(31). Fu R; Miao Y; Qin H; Cross TA Probing Hydronium Ion Histidine NH Exchange Rate Constants in the M2 Channel via Indirect Observation of Dipolar-Dephased ^{15}N Signals in Solid-State Magic-Angle-Spinning NMR. J. Am. Chem. Soc 2016, 138, 15801. [PubMed: 27960325]

(32). Qin H; Miao Y; Cross TA; Fu R Beyond structural biology to functional biology: Solid-state NMR experiments and strategies for understanding the M2 proton channel conductance. J. Phys. Chem. B 2017, 121, 4799. [PubMed: 28425709]

(33). Grabowski SJ What Is the Covalency of Hydrogen Bonding? Chem. Rev 2011, 111, 2597. [PubMed: 21322583]

(34). Dingley AJ; Cordier F; Grzesiek S An Introduction to Hydrogen Bond Scalar Couplings. Concepts Magn. Reson 2001, 13, 103.

(35). Joyce SA; Yates JR; Pickard CJ; Brown SP Density Functional Theory Calculations of Hydrogen-Bond-Mediated NMR J Coupling in the Solid State. J. Am. Chem. Soc 2008, 130, 12663. [PubMed: 18729362]

(36). Blake JB; Adams MWW; Summers MF Novel Observation of NH-S(Cys) Hydrogen-Bond-Mediated Scalar Coupling in ^{113}Cd-Substituted Rubredoxin from Pyrococcus furiosus. J. Am. Chem. Soc 1992, 114, 4931.

(37). Dingley AJ; Grzesiek S Direct observation of hydrogen bonds in nucleic acid base pairs by internucleotide $^{2}J_{NN}$ couplings. J. Am. Chem. Soc 1998, 120, 8293.

(38). Pervushin K; Ono A; Fernandez C; Szyperski T; Kainosho M; Wuthrich K NMR scalar couplings across Watson!Crick base pair hydrogen bonds in DNA observed by transverse relaxation-optimized spectroscopy. Proc. Natl. Acad. Sci. U. S. A 1998, 95, 14147. [PubMed: 9826668]

(39). Cornilescu G; Hu JS; Bax A Identification of the hydrogen bonding network in a protein by scalar couplings. J. Am. Chem. Soc 1999, 121, 2949.

(40). Hennig M; Geierstanger BH Direct detection of a histidinehistidine side chain hydrogen bond important for folding of apomyoglobin. J. Am. Chem. Soc 1999, 121, 5123.

(41). Brown SP; Perez-Torralba M; Sanz D; Claramunt RM; Emsley L Determining hydrogen-bond strengths in the solid state by NMR: the quantitative measurement of homonuclear *J* couplings. Chem. Commun 2002, 1852.

(42). Brown SP; Perez-Torralba M; Sanz D; Claramunt RM; Emsley L The Direct Detection of a Hydrogen Bond in the Solid State by NMR through the Observation of a Hydrogen-Bond Mediated 15N-15N J Coupling. J. Am. Chem. Soc 2002, 124, 1152. [PubMed: 11841267]

(43). Pham TN; Griffin JM; Masiero S; Lena S; Gottarelli G; Hodgkinson P; Filip C; Brown SP Quantifying hydrogen-bonding strength: the measurement of $2h^{J}_{NN}$ couplings in self-assembled guanosines by solid-state ^{15}N spin-echo MAS NMR. Phys. Chem. Chem. Phys 2007, 9, 3416. [PubMed: 17664965]

(44). Miao Y; Cross TA; Fu R Differentiation of histidine tautomeric states using ^{15}N selectively filtered ^{13}C solid-state NMR spectroscopy. J. Magn. Reson 2014, 245, 105. [PubMed: 25026459]

(45). Lesage A; Emsley L; Penin F; Bockmann A Investigation of Dipolar-Mediated Water-Protein Interactions in Microcrystalline Crh by Solid-State NMR Spectroscopy. J. Am. Chem. Soc 2006, 128, 8246. [PubMed: 16787089]

(46). Takegoshi K; Ogura K; Hikichi K A Perfect Spin Echo in a Weakly Homonuclear *J*-Coupled Two Spin-1/2 System. J. Magn. Reson 1989, 84, 611.

(47). van Zijl PCM; Moonen CTW; von Kienlin M Homonuclear *J* refocusing in Echo Spectroscopy. J. Magn. Reson 1990, 89, 28.

Author Manuscript Author Manuscript Author Manuscript Author Manuscript

(48). Cadars S; Lesage A; Trierweiler M; Heux L; Emsley L NMR measurements of scalar-coupling distributions in disordered solids. Phys. Chem. Chem. Phys 2007, 9, 92. [PubMed: 17164890]

(49). Guerry P; Smith ME; Brown SP ^{31}P MAS Refocused INADEQUATE Spin-Echo (REINE) NMR Spectroscopy: Revealing J Coupling and Chemical Shift Two-Dimensional Correlations in Disordered Solids. J. Am. Chem. Soc 2009, 131, 11861. [PubMed: 19645471]

(50). Hughes CE; Reddy GNM; Masiero S; Brown SP; Williams PA; Harris KD M. Determination of a complex crystal structure in the absence of single crystals: analysis of powder X-ray diffraction data, guided by solid-state NMR and periodic DFT calculations, reveals a new 2'-deoxyguanosine structural motif. Chem. Sci 2017, 8, 3971. [PubMed: 28553539]

Author Manuscript Author Manuscript Author Manuscript Author Manuscript

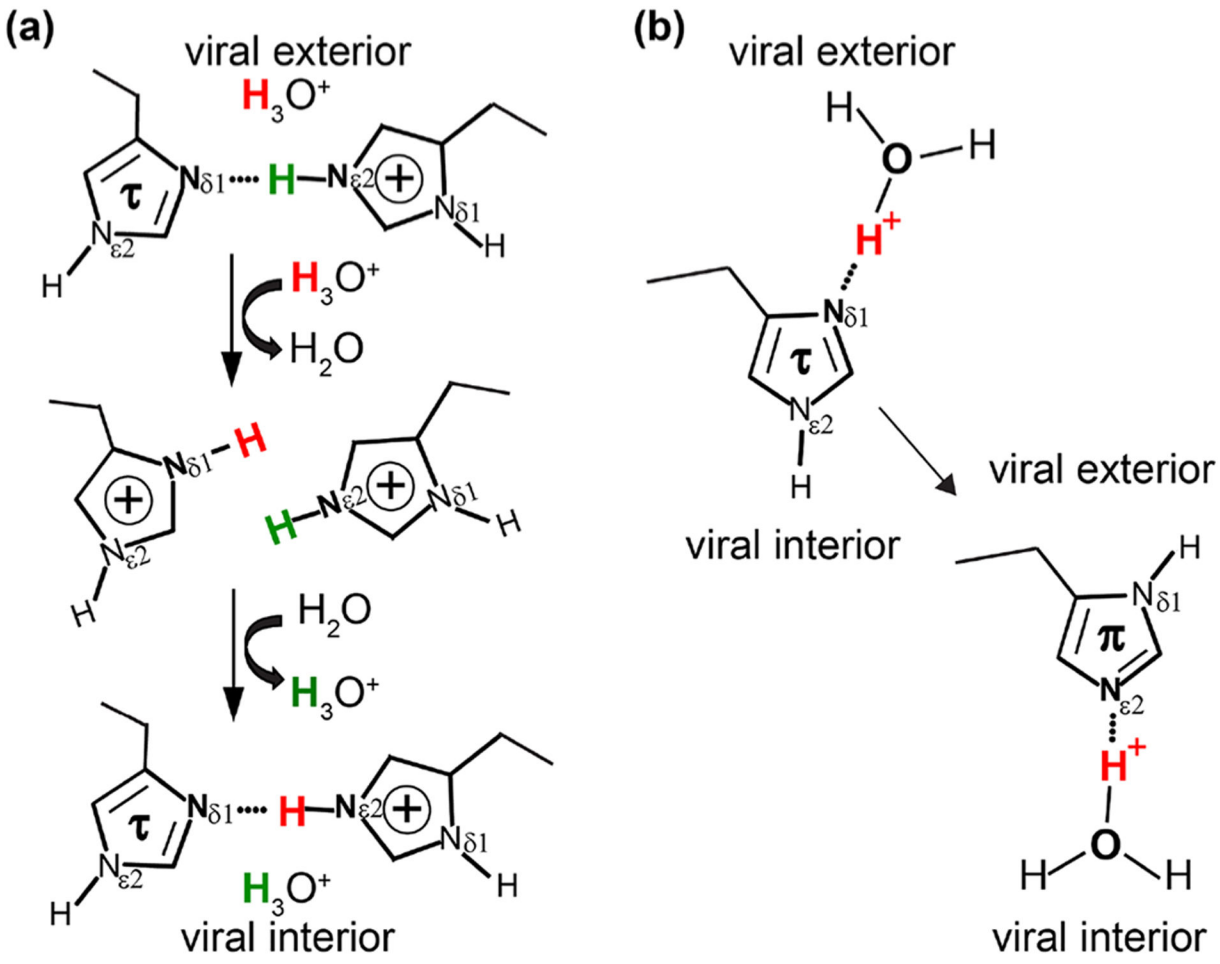

Figure 1.

Two possible hydrogen bonding partnerships in the His37 tetrad of the M2 proton channel. (a) One of two pairs of His37 residues showing the low-barrier hydrogen bond model, in which the proton is transferred through the breaking and reforming of the intermonomer imidazole-imidazolium hydrogen bonds between His37 residues; (b) the water-His37 hydrogen bonding model, in which the His37 shuttles protons through imidazole ring reorientations and exchanging protons with water.

Author Manuscript Author Manuscript Author Manuscript Author Manuscript

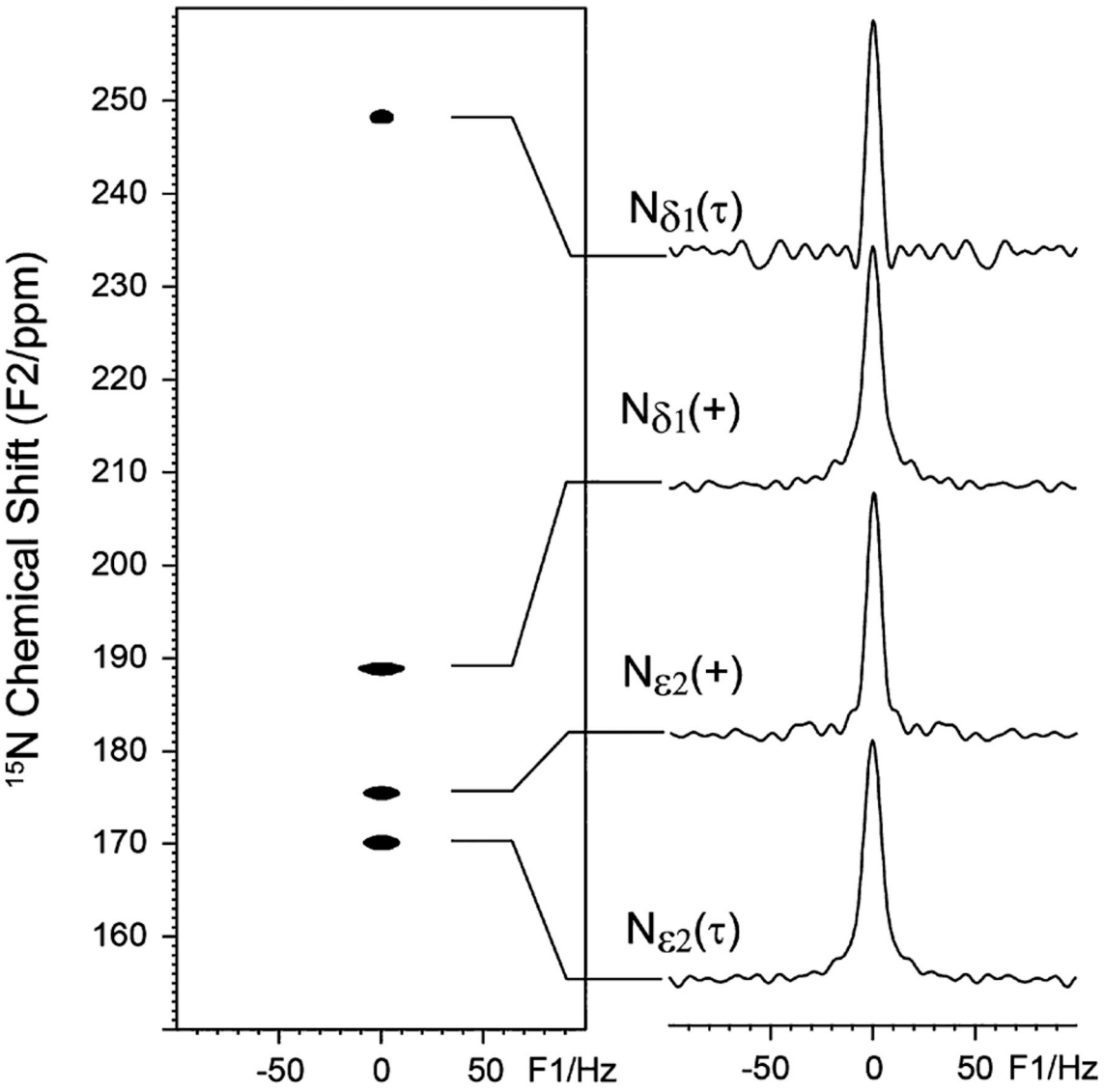

Figure 2.

^{15}N 2D *J*-resolved spectrum (left) of the histidine powder sample (at pH 6.3) and their corresponding slices (right).

Author Manuscript Author Manuscript Author Manuscript Author Manuscript

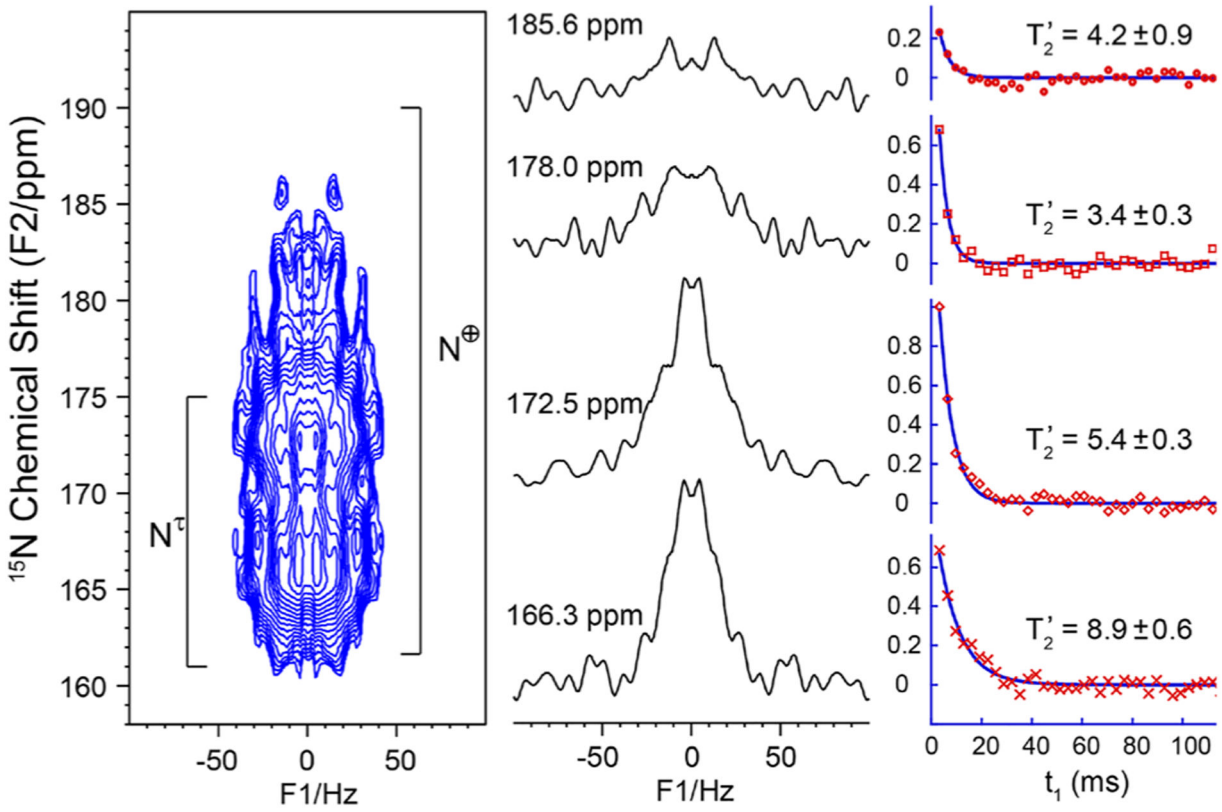

Figure 3.

Expanded ^{15}N 2D *J*-resolved spectrum (left) of the His37-labeled M2FL (pH 6.2) in DOPC/DOPE liposomes and the slices (middle panel) and the normalized echo signal intensities as a function of spin-echo time t_1 (right panel) at different chemical shift positions. This 2D spectrum was recorded in 109 h on a 600 MHz NMR spectrometer where the Larmor frequencies are 600.1 and 60.8 MHz for ^{1}H and ^{15}N, respectively. The sample was spun at 12.5 kHz. The expected protonated ^{15}N chemical shift range for the τ and charge states are marked in the 2D spectrum.

Author Manuscript Author Manuscript Author Manuscript Author Manuscript

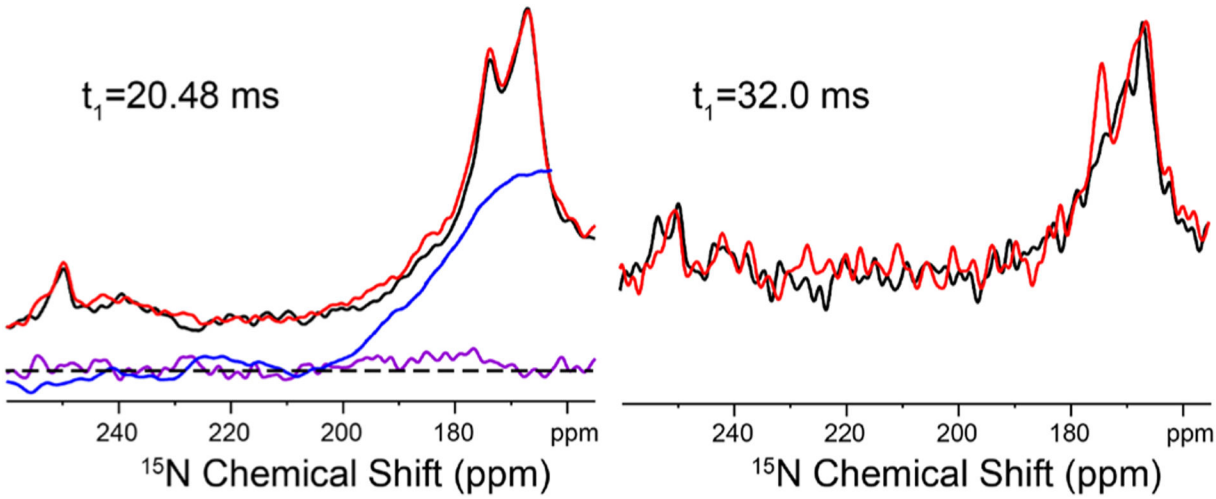

Figure 4.

Expanded ^{15}N doubly spin–echoed spectra of the His37-labeled M2FL (pH 6.2) in DOPC/DOPE liposomes with (red) and without (black) the *J*-refocusing $\pi/2$ pulse at different spin–echo time t_1. The subtraction of the black from red spectra is shown in purple with dashed lines indicating the zero reference. The blue line shows the integration of the difference spectrum from 260 to 164 ppm.